Scientific Reports

https://doi.org/10.1038/s41598-025-29923-1

Article in Press

Hydrothermal carbonization derived hydrochar from industrial waste as an efficient adsorbent for toxic dye removal and process optimization

Received: 14 September 2025

Accepted: 20 November 2025

Published online: 23 January 2026

Cite this article as: Rangasamy G., Rathi B.S., Kumar K.S. *et al.* Hydrothermal carbonization derived hydrochar from industrial waste as an efficient adsorbent for toxic dye removal and process optimization. *Sci Rep* (2026). https://doi.org/10.1038/s41598-025-29923-1

Gayathri Rangasamy, B. Senthil Rathi, K. Sathish Kumar, S. Murugeshwari, S. Meenakshi Lalitha & P. Senthil Kumar

Hydrothermal Carbonization Derived Hydrochar from Industrial Waste as an Efficient Adsorbent for Toxic Dye Removal and Process Optimization

Gayathri Rangasamy[1,2*], B. Senthil Rathi[3,4], K. Sathish Kumar[3,4], S. Murugeshwari[5], S. Meenakshi Lalitha[3,4], P. Senthil Kumar[6*]

[1]Department of Civil Engineering, Faculty of Engineering, Karpagam Academy of Higher Education, Pollachi Main Road, Eachanari Post, Coimbatore-641021, Tamil Nadu, India.
[2]University College, Korea University, Seongbuk-gu, Seoul 02481, Republic of Korea.
[3]Department of Chemical Engineering, Sri Sivasubramaniya Nadar College of Engineering, Chennai-603 110, Tamil Nadu, India
[4]Centre of Excellence in Water Research (CEWAR), Sri Sivasubramaniya Nadar College of Engineering, Chennai-603 110, Tamil Nadu, India
[5]Department of Bioengineering, Institute of Biotechnology, Saveetha School of Engineering, Saveetha Institute of Medical and Technical Sciences, Chennai, 602105, India
[6]Centre for Pollution Control and Environmental Engineering, Pondicherry University, School of Engineering and Technology, Kalapet, Puducherry, 605014, India.

***Corresponding author:** senthilkumarp@pondiuni.ac.in ; senthilchem8582@gmail.com (P. Senthil Kumar);
granga1983@gmail.com **(**Gayathri Rangasamy**)**

Abstract

This study focuses on the removal of Red F2B dye from aqueous solutions using hydrochar prepared from industrial waste via hydrothermal carbonization (HTC). The synthesized hydrochar was thoroughly characterized to assess its structural and surface features (FTIR, XRD, and FESEM-EDS). A series of adsorption trials was performed to examine the influence of pH, temperature, contact time, dye concentration, and hydrochar dosage on dye elimination efficiency. The results indicated that dye removal was highly dependent on pH, achieving optimal removal at pH 3, and that it exhibited endothermic characteristics. The adsorption equilibrium data aligned well with the Langmuir model, with a calculated maximum adsorption capacity of 44.24 mg/g. Kinetic modeling suggested a pseudo-second-order mechanism, indicating that chemisorption governed the adsorption rate. Thermodynamic evaluations confirmed that the process was spontaneous and energy-absorbing. Process optimization was performed using Response Surface Methodology (RSM), which identified pH, hydrochar dose, contact time, and initial dye concentration as key influencing factors. Overall, this study demonstrates the feasibility of utilizing HTC-derived hydrochar from industrial sludge as a sustainable and efficient adsorbent for dye-contaminated wastewater, promoting circular economy and resource recovery concepts.

Keywords: Adsorption; Hydrochar; Industrial sludge; Isotherm; Hydrothermal carbonization.

1. Introduction

The release of synthetic dyes from industries such as textiles, leather, and dye manufacturing has a profound and complex negative impact on environmental health, primarily due to their significant discharge into both aquatic and terrestrial ecosystems. These dyes frequently contain complex aromatic compounds, heavy metals, and other toxic substances that resist natural breakdown, leading to persistent environmental pollution and the risk of bioaccumulation (Routoula & Patwardhan, 2020). When released into water bodies, these dyes impose intense coloration and can severely disrupt aquatic ecosystems by reducing light penetration, impeding photosynthesis, lowering oxygen levels, and impairing food webs (Zahuri et al., 2023). Microbial degradation of organic dye compounds consumes dissolved oxygen (DO) in water, leading to hypoxic or anoxic conditions in the water. Oxygen depletion adversely affects aerobic aquatic organisms, enhancing the risk of fish mortality and dead zones (Vaghela et al., 2005). The presence of dyes in water also diminishes its aesthetic quality, rendering it unsuitable for various applications (Pereira & Alves, 2012). In addition, the production and disposal of dyes leads to pollution of air and soil, introducing harmful chemicals and heavy metals into the environment. These substances can induce acute and chronic toxicity, causing physiological and genetic damage in aquatic species, including reproductive failure, altered behavior and mortality (Luba et al., 2023). The release or leakage of waste containing dyes into the soil can modify its physicochemical characteristics, including pH and nutrient availability. Dyes can disrupt the native microbial consortia that are essential for soil health, impairing plant growth and crop productivity (Zheng et al., 2023).

Many dyes are toxic, persistent, bioaccumulative, and biomagnified, posing long-term dangers to aquatic life and human health. To reduce the environmental effects of industrial dyes, efficient treatment methods must be developed and more stringent regulations on dye application and wastewater management in industrial settings must be implemented.

Adsorption is a process in which molecules, atoms, or ions, collectively referred to as adsorbates, adhere to the surface of a solid material (adsorbent). The principles of adsorption include surface area, selectivity, reversibility, temperature dependence, pressure influence, concentration effects, pH sensitivity, kinetics, equilibrium, surface chemistry, pore size distribution, and competitive adsorption. Understanding these principles is crucial for creating efficient adsorption processes in a range of applications, including water and gas purification and catalysis (Sukmana et al., 2021). Compared to methods that require

expensive reagents or infrastructure, adsorption can be performed using natural or low-cost materials, making it economically viable for large-scale applications. Adsorption reduces the production of secondary pollutants and eliminates the need for additional chemicals, thereby lowering the possibility of additional water resource contamination. It can be integrated with other treatments, such as electrocoagulation, to enhance overall treatment efficiency (Graça & Rodrigues, 2022).

Hydrochar is increasingly recognized for its effectiveness in adsorbing various water pollutants, including dyes. Its structure, characterized by high porosity and a large specific surface area, offers numerous sites for the adsorption of dyes. The pore size varies from micropores to macropores, enabling both surface adsorption and intraparticle diffusion. The surface of hydrochar is rich in oxygen-containing functional groups, including carboxyl, hydroxyl, and phenolic groups, which can interact with dye molecules through mechanisms such as hydrogen bonding, electrostatic attraction, and π-π interactions (Kapoor et al., 2022). Hydrochar's ability to efficiently eliminate dyes from water solutions is attributed to a blend of physical adsorption and chemical interactions. Its impressive adsorption capacity and eco-friendly nature position hydrochar as a promising option for water treatment. Huge quantities of sludge are discharged every year by various industries, raising serious environmental concerns. The recovery and reuse of sludge for sustainable management must be encouraged to reduce its impact on the environment. Sludge-derived biochar has been successfully used in wastewater treatment to remove various pollutants through adsorption and catalytic reactions. Its high surface area, porosity, and functionality enable the removal of heavy metals and organic pollutants, contributing to its effectiveness in wastewater purification (Zhou et al., 2024).

Despite numerous studies on hydrochar derived from different biomass and sludge sources, research focusing on the hydrothermal carbonization (HTC) of industrial sludge, specifically from textile wastewater streams, remains limited. The influence of the sludge source, processing method, particularly HTC, and activation strategies on the physicochemical properties and adsorption efficiency of hydrochar remain poorly understood. Most studies favor conventional pyrolysis for sludge biochar synthesis, while the application of HTC, a milder, energy-efficient alternative to industrial textile sludge, remains underexplored.

In this study, industrial sludge from a textile manufacturing facility was used as feedstock to synthesize hydrochar via HTC. This approach allows the generation of hydrochar with distinct surface functionalities that are favorable for dye adsorption. Unlike previous studies (Jellali et al., 2022; Raj et al., 2021) that primarily relied on pyrolyzed sludge biochars involving high temperature, this study integrates Response Surface Methodology (RSM) for the systematic optimization of key operational parameters influencing the adsorption of Red F2B dye.

This study aimed to thoroughly analyze the physicochemical characteristics of hydrochar produced through HTC and evaluate its ability to adsorb pollutants from aqueous solutions. Furthermore, this study examined the effectiveness of hydrochar in treating Red F2B dye and compared its performance with that of traditional adsorbents typically used in wastewater treatment. This detailed approach provides insights into both the fundamental properties and practical use of HTC-derived biochar in environmental cleanup. This study presents an innovative method that utilizes industrial waste as an eco-friendly and economical source for producing hydrochar, thereby addressing the environmental challenges associated with waste accumulation and water pollution. The combination of waste valorization and wastewater treatment supports the principles of a circular economy, fostering comprehensive and sustainable environmental solutions for the future. This approach also presents a budget-friendly and environmentally sustainable alternative to conventional adsorbents such as activated carbon. The results of this study have considerable potential to enhance wastewater treatment. The improved pollutant removal efficiency of HTC-synthesized biochar could lead to lower treatment costs and reduced energy use, making wastewater management more economical and sustainable than conventional methods. Expanding the range of adsorbent materials helps decrease the reliance on conventional options, such as activated carbon, while promoting resource recovery from industrial waste streams. The feasibility of producing and applying hydrochar on-site within industrial facilities further enhances operational efficiency. Moreover, converting waste into high-value adsorbents can help industries reduce disposal costs and meet increasingly strict environmental regulations. These advantages collectively pave the way for the development of new business models focused on waste-derived materials and sustainable treatment technologies.

2. Materials and Methods

2.1. Chemical Reagents

Industrial sludge was obtained from Pioneer Jellice India Pvt. Ltd., manufacturing facility in Cuddalore, for hydrochar preparation. The red F2B dye was purchased from a local dyeing facility. Sodium Hydroxide (NaOH), Hydrochloric acid (HCl) and other chemicals used were standard analytical grade

2.2. Adsorbate Preparation

Red F2B (C.I. Reactive Red 194- $C_{27}H_{18}C_1N_7Na_4O_{16}S_5$; MW: 984.21 g/mol) is a single-azo anionic reactive dye commonly used in textile dyeing. Its chemical structure consists of an extended aromatic ring system connected to sulfonate and amino groups along with triazine rings that serve as reactive sites. Its molecular structure is shown in **Figure *1***. A stock solution of 1000 mg/L was prepared and diluted for the working solution.

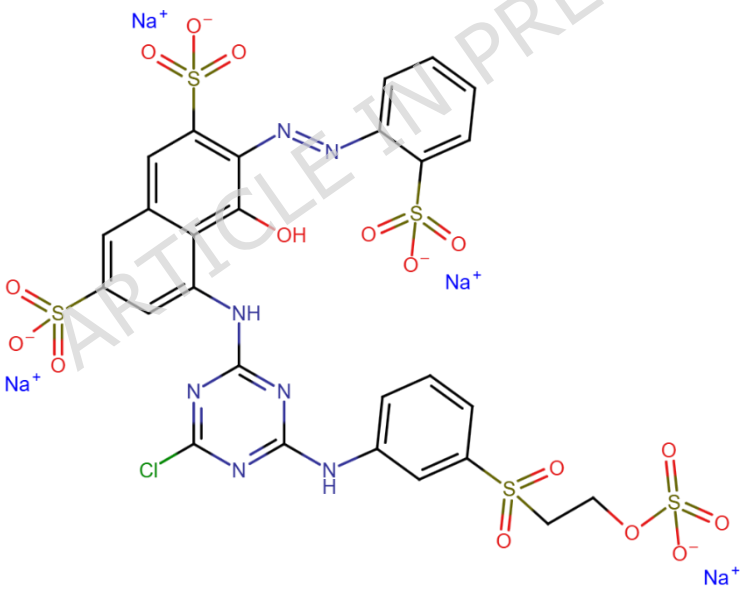

Figure 1. Structure of Reactive Red 194 dye

2.3. Preparation of HTC- synthesized Hydrochar

A total of 100 g of industrial sludge was collected, spread out in a tray, and dried at 90 °C for 4 h. After drying, the solids were ground into a fine powder. In an autoclave reactor, 3 g of dried sludge was combined with 75 ml of water. The mixture was then placed in a hot-air

oven at 180 °C for 18 h. Subsequently, the HTC reactor was allowed to cool, and the contents were filtered to produce hydrochar. The solids were dried in a hot-air oven and stored in an airtight container. To 3 g of prepared hydrochar, 0.05 M concentrated H_2SO_4 was added and stirred using a magnetic stirrer with the temperature maintained at 50 ℃ for 4h. After activation, the hydrochar was filtered and washed multiple times until neutralization was achieved. The hydrochar was then dried and stored for future use (2).

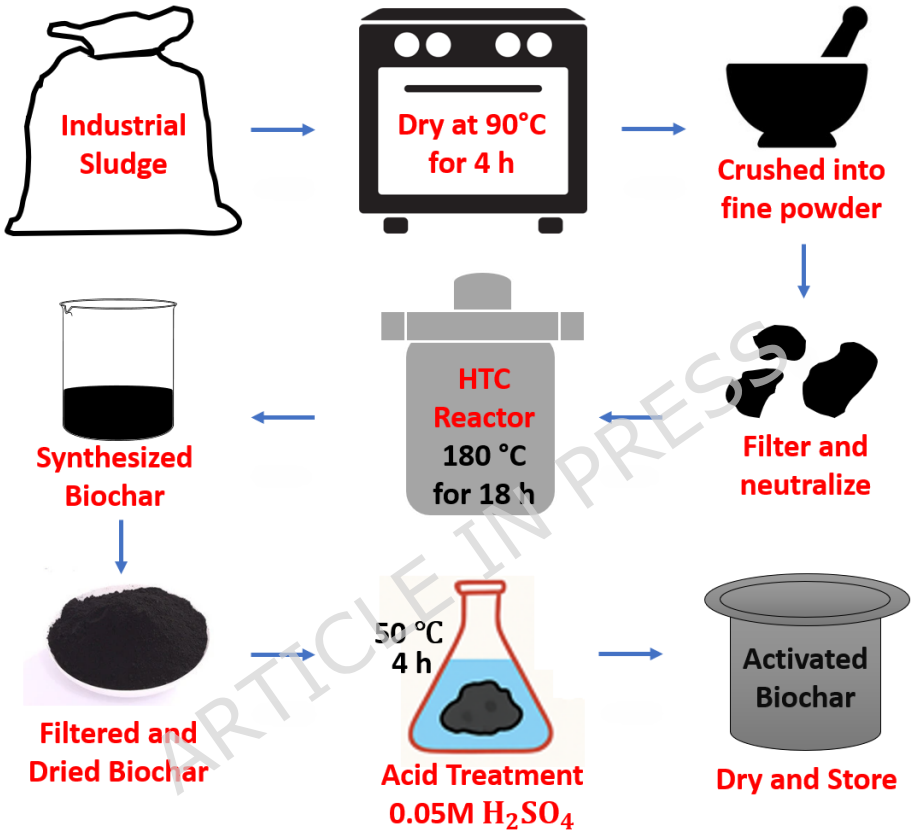

Figure 2. Methodology for synthesis of Activated hydrochar

2.4. Analytical Methods

The physicochemical properties were estimated using standard proximate analysis method. The moisture content of the sample was assessed by heating it at 105 °C until its weight remained constant. The volatile matter of the sample was determined by subjecting it to a temperature of 900 °C without the presence of oxygen for a set period. The ash content of the sample was measured by burning it at 750 °C in a muffle furnace. The fixed carbon content was calculated by deducting the total of moisture, volatile matter, and ash from 100%.(Jian et al., 2018).

The hydrochar synthesized from industrial sludge through hydrothermal carbonization was characterized to evaluate its structural, morphological, and chemical properties using several techniques. The functional compounds on the hydrochar surface were analyzed using an FT/IR-6X spectrophotometer (JASCO, Japan), recording spectra at 4000–400 cm^{-1} using the KBr pellet method. The absorption bands obtained were interpreted to identify the surface functionalities that might contribute to dye adsorption. The crystallographic properties of the hydrochar were evaluated using an Empyrean X-ray diffractometer (Malvern PANalytical, Netherlands) with a copper anode (λ = 1.5406 Å). To assess the crystallinity and identify the mineral phases, diffraction patterns were captured across a 2θ range of 10°–80°, with increments of 0.02°, using settings of 40 kV and 30 mA. The surface morphology and microstructural characteristics of the hydrochars were analyzed using a high-resolution Apero 2S FESEM. To improve the conductivity, the samples were coated with gold prior to imaging. Images were captured at various magnifications to observe the porosity, surface roughness, and particle arrangement. To verify the elemental composition of the hydrochar, energy-dispersive X-ray spectroscopy (EDS) was employed in conjunction with FESEM for elemental analysis. A double-beam UV-visible spectrophotometer (M/s. Lark) was employed to assess the dye concentration both prior to and after the adsorption experiments. The wavelength at which the Red F2B dye exhibited maximum absorbance (λ_{max}) was identified, and standard calibration curves were created to measure the dye concentration in solution.

2.5. Adsorption Experiments

To evaluate the adsorption capabilities of the synthesized hydrochar for eliminating Red F2B dye from water solutions, batch adsorption tests were performed. These experiments were performed in 100 mL conical flasks under controlled laboratory conditions. A stock solution of Red F2B dye (1000 mg/L) was prepared by dissolving an accurately measured amount of dye in distilled water. Working solutions with desired concentrations (5, 10, 15, and 20 mg/L) were prepared by diluting the stock solution with double-distilled water. A 50 mL dye solution was combined with the required quantity of hydrochar and stirred on an orbital shaker at 150 rpm for a predetermined time. Following the adsorption process, the mixtures were filtered to remove the adsorbent, and the remaining dye concentration in the supernatant was measured at the peak absorbance wavelength (540 nm) of Red F2B dye. To explore the impact of various operational parameters on adsorption efficiency, the following conditions were systematically varied: contact time: 10, 20, 30, 40, 50, and 60 min; solution

temperature: 30, 40, 50, and 60 °C; initial pH: 3, 5, 7,9 and 11 (adjusted using 0.1 N HCl or NaOH); adsorbent dose: 0.2, 0.4, 0.6, and 0.8 g/L; and initial dye concentration: 5, 10, 15, and 20 mg/L. To assess the impact of each parameter on the adsorption process, each parameter was examined separately while the others were held constant.

The equilibrium adsorption capacity (q_e, mg g^{-1}) and percentage dye removal were calculated using the following equations,

$$q_e = \frac{(C_0 - C_e) * V}{m} \#(1)$$

$$\text{Removal } (\%) = \frac{(C_0 - C_e)}{C_0} * 100 \#(2)$$

where C_0 is initial dye concentration, C_e is equilibrium dye concentration (mg/L), V is volume of dye solution (L) and m is mass of hydrochar (g). The findings from these experiments were used to examine the adsorption kinetics, isotherms, and thermodynamic parameters.

2.6. Isotherm, Kinetics and Thermodynamic Data Modelling

To comprehend the adsorption mechanism and its features, adsorption isotherm, kinetics, and thermodynamic data were examined using a range of models. The equilibrium data were fitted to Langmuir (LI), Freundlich (FI), and Temkin (TI) isotherm models to identify the most suitable model and to compute key parameters, such as the maximum adsorption capacity and adsorption intensity.

a) Langmuir Isotherm

$$q_e = \frac{q_{max} K_L C_e}{1 + K_L C_e} \#(3)$$

The separation factor was calculated using formula,

$$R_L = \frac{1}{1 + bC_0} \#(4)$$

where R_L is the separation factor, b is the Langmuir constant related to the adsorption energy (L mg^{-1}), and C_0 is the initial adsorbate concentration (mg L^{-1}). The value of R_L indicates adsorption favorability.

b) Freundlich Isotherm (FI)

$$q_e = K_F C_e^{1/n} \#(5)$$

c) Temkin Isotherm (TI)

$$q_e = \frac{RT}{b} \ln(AC_e) \#(6)\#$$

where q_{max} and q_e are maximum adsorption capacity and adsorption capacity at equilibrium (mg g^{-1}) respectively; C_e is equilibrium dye concentration (mg L^{-1}); n is the Freundlich exponent; K_L (L mg^{-1}) and K_F (mg/g) $(L/mg)^{\frac{1}{n}}$ are the constants of the respective isotherm models, R universal gas constant (8.314 J/mol K), T temperature (K), b constant related to heat (J mol^{-1}), C_e is equilibrium adsorbate concentration (mg L^{-1}) and A Temkin constant (L mg^{-1}).

Kinetic data were evaluated using pseudo-first-order (PFO), pseudo-second-order (PSO), and intraparticle diffusion (IPD) models to elucidate the rate-controlling steps and adsorption rates.

a) PFO

$$q_t = q_e(1 - e^{-K_1 t}) \#(7)$$

b) PSO

$$q_t = \frac{K_2 q_e^{\,2} t}{1 + K_2 q_e t} \#(8)$$

c) IPD

$$q_t = K_{id}\, t^{0.5} + C \#(9)$$

where q_t (mg g^{-1}) amount of dye adsorbed at time t (min), a represents the equilibrium adsorption capacity (mg g^{-1}), b is the rate constant (min^{-1}), q_e (mg g^{-1}) is the equilibrium

adsorption capacity, K_1 (min^{-1}) and K_2 (g mg^{-1} min^{-1}) is the PSO rate constant, $t^{0.5}$ square root of time ($min^{0.5}$), K_{id} intraparticle diffusion rate constant (mg/g·$min^{0.5}$) and C (mg g^{-1}) intercept related to boundary layer thickness.

Thermodynamic parameters, including Gibbs free energy change (ΔG°), enthalpy change (ΔH°), and entropy change (ΔS°), were calculated using the Van't Hoff equation to evaluate the spontaneity, heat change, and randomness of the adsorption process.

$$\ln K_C = -\frac{\Delta H^\circ}{R}\cdot\frac{1}{T} + \frac{\Delta S^\circ}{R} \quad \#(10)$$

$$\Delta G = \Delta H - T\Delta S \quad \#(11)$$

where K_C is the adsorption capacity, ΔS is change in entropy (J/mol·K), ΔH is change in enthalpy(J/mol), R is universal gas constant (8.314 J/mol·K) and T is temperature in Kelvin.

All model fittings and parameter estimations were performed using non-linear regression analysis in statistical software, with the coefficient of determination (R^2) and root mean square error (RMSE) used to evaluate goodness of fit.

2.7. RSM Optimization

To enhance the efficiency of dye removal using hydrochar derived from industrial solid waste, a linear model was employed using Response Surface Methodology (RSM).A total of 35 experimental runs with varying levels of five independent variables—pH (A), temperature (B), hydrochar dosage (C), contact time (D), and initial dye concentration (E) were used to develop the model (**Table 1**). Design-Expert software (version 12) was used for the regression analysis, ANOVA, and response surface generation. The response variable was removal efficiency (%).

Table 1. Variable levels Considered for Red F2B dye by Activated Hydrochar

S.No.	Factor	Name	Variable Level	
			-1	+1
1	A	pH	3	11
2	B	Temperature (K)	303	333
3	C	Hydrochar Dosage (g/L)	0.2	0.8
4	D	Time (min)	10	60
5	E	Dye concentration (mg/L)	5	20

3. Results and Discussion

3.1. HTC-synthesized hydrochar

To assess the fundamental composition of the hydrochar, a proximate analysis was performed, focusing on the moisture content, volatile matter, ash content, and fixed carbon. These factors are essential for evaluating fuel value, adsorption capacity, and thermal properties of hydrochar. The findings are presented in **Table 2**.

Table 2. Proximate analysis of HTC hydrochar derived from industrial sludge

Parameter	Value (g)	Percentage (%)
Moisture Content	47.5 g	47.5%
Volatile Matter	~20 g	~20%
Ash Content	~7.5 g	~7.5%
Fixed Carbon	~25 g	~25%

The hydrochar demonstrated a fairly high moisture level of 47.5%, which is common for solids derived from HTC owing to the wet processing technique. The volatile matter content of approximately 20% suggests the presence of organic components that can decompose, potentially affecting the surface chemistry during adsorption (Wang et al., 2020). With a fixed carbon content of approximately 25%, biochar is rich in carbon, underscoring its effectiveness as a carbon-based adsorbent (Chen et al., 2021). The ash content, approximately 7.5%, indicates the presence of inorganic residues, which may also play a role in surface interactions with the dye (Wang et al., 2020). These findings affirm the appropriateness of HTC biochar for adsorption applications, particularly given the balance between carbon content and surface-active elements.

FTIR was used to examine the surface functional compounds on the synthesized hydrochar. The corresponding spectra are shown in **Figure *3*3.** The broad absorption bands observed at 3515.50 cm^{-1} and 3398.98 cm^{-1} can be attributed to the O–H stretching vibrations of hydroxyl groups, indicating the presence of alcohols or phenolic compounds, which contribute to hydrogen bonding interactions during adsorption (Mccall et al., 2024). A moderate band at 1684.84 cm^{-1} is indicative of the C=O stretching vibrations of carboxylic acid or carbonyl groups, indicate the retention of oxygenated functionalities within the hydrochar. Additionally, a distinct peak at 1620.44 cm^{-1} is likely due to C=C stretching in aromatic rings, suggesting the partial aromatic nature of the carbonaceous matrix (Veiga et

al., 2017). The pronounced peak at 1105.28 cm^{-1} corresponds to the C–O stretching vibrations found in alcohols, esters, and ethers. These functional groups, which contain oxygen, increase surface polarity of hydrochar and promote both electrostatic and chemical interactions with dye molecules during the adsorption process. (Pasieczna-Patkowska et al., 2025). Collectively, these functional compounds provide abundant active sites for adsorption. The O–H, C=O, C=C, and C–O groups present on the hydrochar surface are critically linked to the adsorption of Red F2B dye via hydrogen bonding, electrostatic attraction, and π–π stacking interactions.

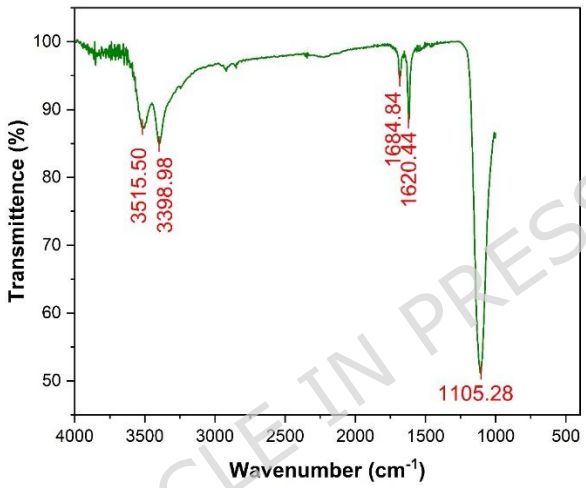

Figure 3. FTIR Analysis of Activated Hydrochar

An XRD plot of the synthesized hydrochar is shown in **Figure *4*. XRD pattern of activated hydrocharFigure *44*,** displaying several sharp, well-defined peaks at 2θ values of 11.92°, 21.01°, 23.63°, 29.38°, 31.38°, and 33.64°, with peak intensities ranging from approximately 200 to 800 arbitrary units. This lower-angle peak often corresponds to larger d-spacing values, which can signify the presence of organic or less-ordered amorphous phases common in hydrochar derived from plant materials, such as cellulose or lignin derivatives (Yoo et al., 2018). These amorphous regions provided a porous structure with accessible surface sites for dye molecules, promoting enhanced adsorption via physical entrapment and diffusion. The intense peaks at 21.01° and 23.63° are characteristic of cellulose-related structures. These peaks are typical of semicrystalline cellulose, with diffraction patterns reflecting the arrangement of cellulose chain planes (Kaliyamoorthy et al., 2025). These domains increase the textural complexity and surface area, facilitating greater accessibility of the adsorption sites for dye molecules. The peaks at 29.38° signify mineral matter, such as calcium

carbonate (calcite), often found within hydrochar containing mineral additives or derived from biomass with high mineral content originating from industrial sludge and mineral-rich precursors (Andersen et al., 2005). Calcite sites are known to support adsorption processes through surface complexation and potential ion-exchange interactions with dye molecules, especially those possessing anionic functional groups. The diffraction peaks at 31.38° and 33.64° are typically indicative of the presence of more ordered graphitic domains formed within the hydrochar owing to the elevated temperature. Higher carbonization temperatures lead to increased graphitization, which typically appears in the XRD pattern at higher angles (Khan et al., 2020). These domains enhance the electrical conductivity of hydrochar and provide π-electron-rich surfaces that can interact with aromatic dye rings through π–π stacking. This structural feature further strengthens the adsorption mechanism of dyes with aromatic cores.

Overall, the XRD pattern suggests that the synthesized hydrochar had a complex structure comprising organic, amorphous, and likely mineral phases as well as graphitic layers. Each component contributes synergistically to the adsorption mechanism: the amorphous and cellulose phases promote physical adsorption and surface accessibility. Mineral phases (e.g., calcite) enable chemical binding and ion exchange, and graphitic domains facilitate π–π interactions with dye molecules (Zhang et al., 2020).

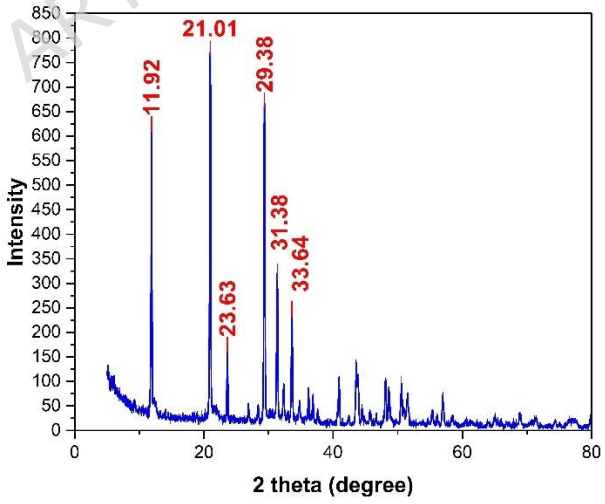

Figure 4. XRD pattern of activated hydrochar

The FESEM micrograph (**Figure *5*5Figure *5*** reveals a highly heterogeneous and porous structure characteristic of HTC-derived hydrochar materials (Liang et al., 2016). The hydrochar exhibited a complex surface structure characterized by irregularly distributed

pores of various sizes, ranging from micropores to macropores, consistent with findings reported for similar hydrothermal carbonization processes (Hossain et al., 2020). The porous architecture demonstrates the 3D interconnected pore network that develops during the HTC process owing to the release of volatile organic compounds and water vapor (Fahmi et al., 2018). At higher magnifications, the hydrochar surface displayed well-defined tubular and cylindrical pore structures alongside slit-like cavities that are characteristic of lignocellulosic biomass-derived materials (Ali et al., 2023). These structural features are attributed to the preservation of the original biomass cellular architecture during relatively mild HTC conditions (Petrovic et al., 2024). Overall, FESEM analysis confirmed that the structural attributes of the activated hydrochar were favorable for effective adsorption of Red F2B dye.

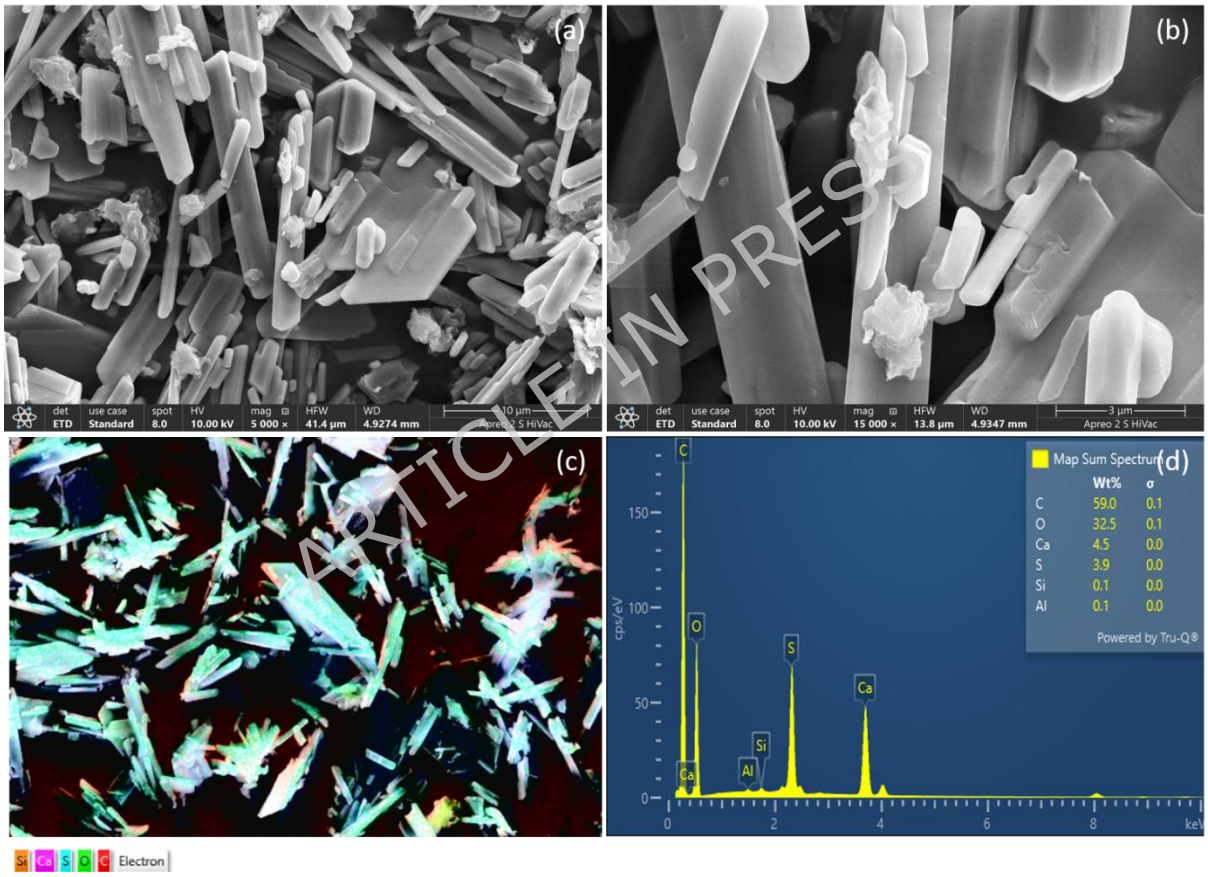

Figure 5. Surface morphology and elemental analysis of the hydrochar sample a) FESEM image at 10 µm magnification; b) FESEM image at 3 µm magnification; c) Coated FESEM image with EDX mapping; d) EDX spectrum showing elemental composition

EDS characterization of the activated hydrochar showed a dominant carbon content (59.0 wt%), indicative of successful carbonization. Oxygen (32.5 wt%) suggests the presence of oxygenated surface functional groups. These abundant functionalities are known to enhance the adsorption capability of hydrochar by facilitating interactions with various pollutants

through hydrogen bonding, electrostatic attractions, and surface complexation. Additionally, inorganic elements, including calcium (4.5 wt. %) and sulfur (3.9 wt. %), were identified, along with trace amounts of silicon and aluminum (<0.2 wt. % combined). The presence of these mineral constituents is consistent with the original biomass feedstock and hydrothermal process parameters, which typically retain mineral matter within the biochar structure (Libra et al., 2011). These inorganic elements may contribute to the functionality of the adsorbent by providing additional active sites and promoting ion-exchange interactions (Qambrani et al., 2017).

EDS analysis revealed that HTC biochar featured diverse surface chemistry, characterized by a carbon-oxygen framework enriched with minerals, highlighting its potential effectiveness as an adsorbent for environmental cleanup applications.

3.2. Influence of operational parameters on Red F2B adsorption

3.2.1. Influence of pH on Red F2B adsorption

The effect of the initial pH on the dye removal efficiency was assessed across a pH spectrum of 3–11. The results clearly demonstrate that the removal efficiency is influenced by the initial pH of the solution (**Figure *6*6**). At pH 3, the dye removal efficiency reached a peak of 83%. As the pH increased to 5 and 7, the removal efficiencies were 62-63%, showing minimal variation between these two pH levels. When the pH was further increased to 9 and 11, there was a notable reduction in removal efficiency, which fell to 45.49% at pH 11. This trend aligns with the expected behavior of anionic dye adsorption onto adsorbents, especially those with variable surface charges. The significant impact of pH on dye adsorption arises from alterations in the surface charge of the adsorbent and the ionization state of the dye molecules. Red F2B contained multiple sulfonate ($–SO_3^-$) groups that remained ionized over the tested pH range (3–11), ensuring that the dye remained predominantly anionic. Thus, the pH-dependent adsorption efficiency is governed by the interplay between the persistent negative charge of the dye and pH-responsive surface charge of the hydrochar adsorbent. When the pH is low, the adsorbent surface becomes heavily protonated and gains a strong positive charge. This results in a strong electrostatic attraction between the positively charged adsorbent and negatively charged dye anions, leading to optimal removal efficiency (Hashim et al., 2019). When the pH is nearly neutral, the surface of the adsorbent approaches its point of zero charge (PZC), leading to a surface that is almost neutral. Electrostatic forces are relatively weak; thus, the removal efficiencies at pH 5 and 7 are nearly identical

(approximately 62-63%). This plateau is consistent with findings reported, Congo Red removal remained nearly constant between pH 5 and 7, attributed to the proximity to the PZC (Wei et al., 2022).

Non-electrostatic interactions such as hydrogen bonds and π–π stacking play a more prominent role in adsorption under these conditions. When the pH level is high, the surface of the adsorbent acquires a negative charge, resulting in electrostatic repulsion with anionic dye species. Competing hydroxide ions (OH^-) may further interfere with dye adsorption by occupying the active sites on the adsorbent. The removal efficiency decreased significantly at these pH levels, similar to the patterns observed in recent adsorption studies of anionic dyes on bio-based and polymeric adsorbents (Zhao et al., 2023). These data underscore the importance of pH control for optimizing dye removal from wastewater. This behavior closely follows the pH-dependent zeta potential of hydrochar, transitioning from positive/neutral under acidic conditions to negative at high pH owing to deprotonation of the surface –OH and –COOH groups. Recent studies on various adsorbents and anionic dyes consistently confirmed that dye removal is maximized at acidic pH, decreases gradually near the PZC, and decreases sharply under alkaline conditions. The plateau effect at pH 5–7 is a well-documented phenomenon in 2023–2025 studies on both bio-based and synthetic adsorbents, highlighting that surface charge neutrality translates to a minimal electrostatic force for dye adsorption within this pH range (Sudarsan et al., 2025).

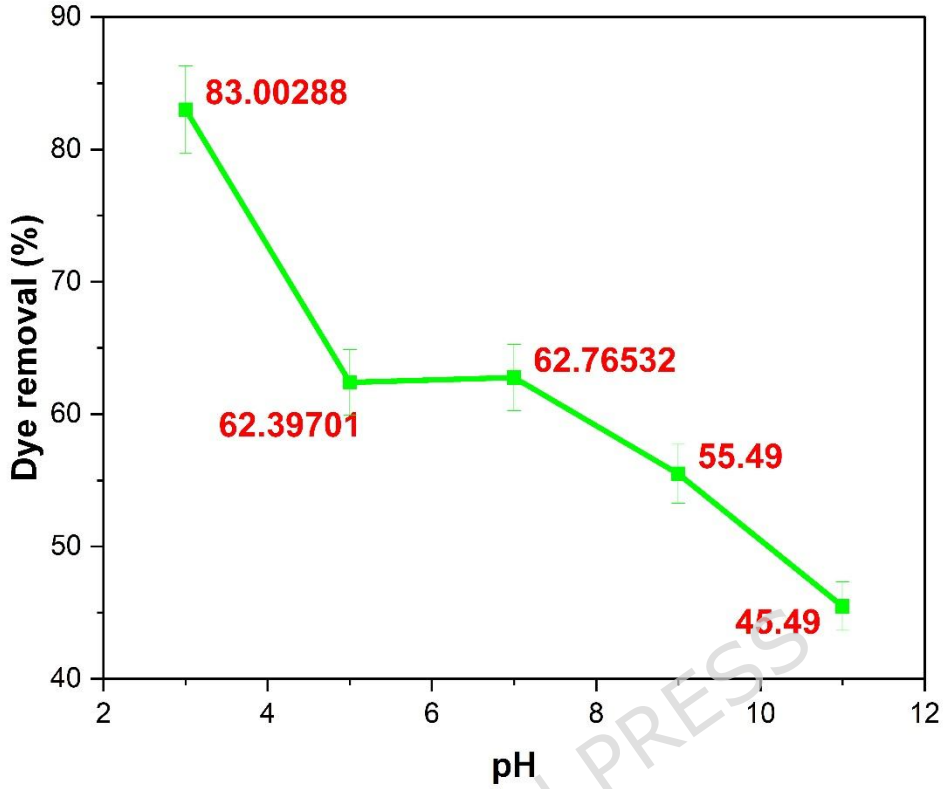

Figure 6. Influence of pH on Red F2B adsorption

3.2.2. Influence of temperature on Red F2B adsorption

The adsorption experiments revealed a clear positive correlation between temperature and dye removal efficiency, with removal rates increasing from 72.4% at 30 °C to 93.3% at 60 °C (**Figure** *7*7). This upward trend indicates that the adsorption process is endothermic, as the increase in thermal energy boosts dye adsorption on the hydrochar surface. (Budnyak et al., 2020). The enhanced dye adsorption at elevated temperatures can be explained by several factors: the dye molecules gain more kinetic energy, resulting in more frequent and effective interactions with the adsorbent surface; the hydrochar structure may experience pore size expansion, facilitating better dye penetration; and additional adsorption sites might become active at higher temperatures. The substantial improvement in removal efficiency indicates that temperature plays a crucial role in optimizing the adsorption process for this activated hydrochar-dye system. Elevated thermal energy can also expand existing pores or create new active sites by weakening or breaking weaker bonds on the hydrochar surface, thereby increasing the number of available adsorption sites (Smoczyński et al., 2020). The

temperature range of 30–60 °C was deliberately chosen to simulate realistic wastewater treatment conditions and to ensure the thermal stability of the hydrochar, as higher temperatures may alter its surface chemistry or cause the desorption of bound dye molecules.

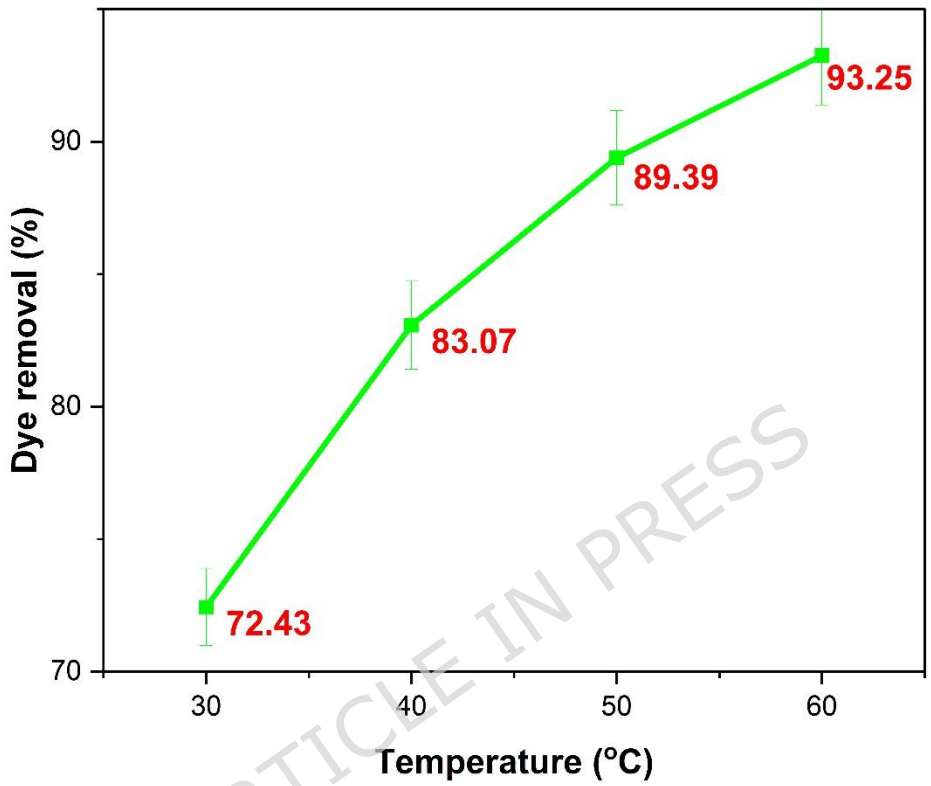

Figure 7. Influence of temperature on Red F2B adsorption

3.2.3. Influence of time on Red F2Badsorption

The adsorption experiments demonstrated a classic two-stage uptake profile: a rapid initial phase followed by a slower approach to equilibrium. Within the first 10 min, the dye removal was approximately 21.03%, reflecting the abundance of available sites and strong driving forces for mass transfer. Between 10 and 40 min, the removal efficiency rises steeply from 21.03% to 82.37% as the remaining pore surfaces fill. After 40 min, the rate of increase diminished, reaching 97% at 60 min, indicating that most of the active sites were occupied and that the system was nearing equilibrium (**Figure *8***).

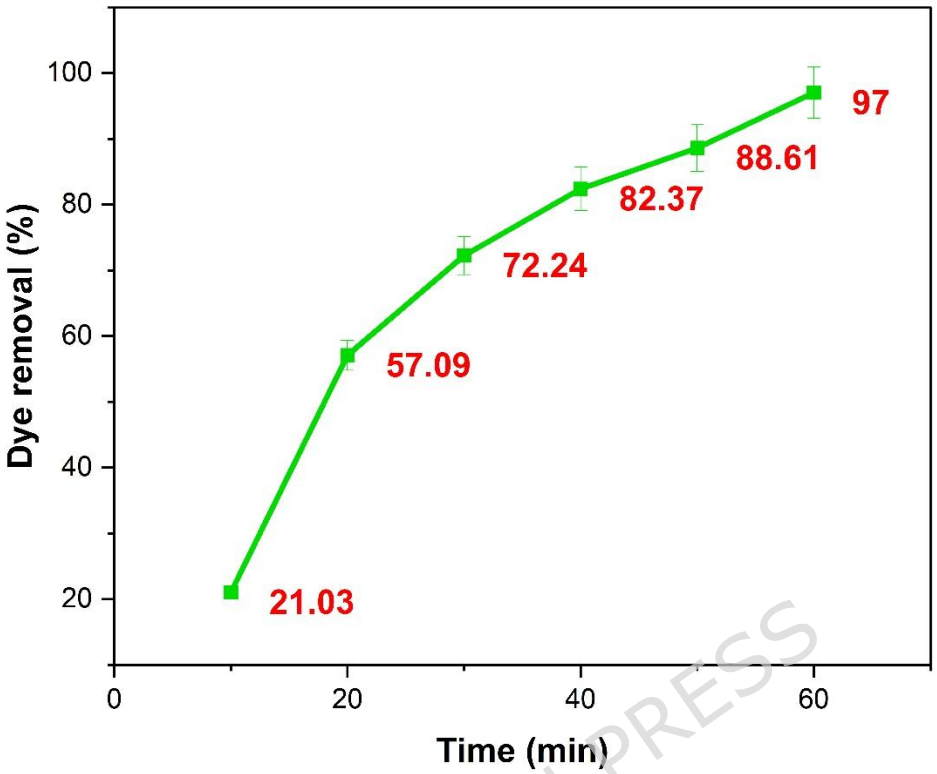

Figure 8. Influence of time on Red F2B adsorption

This behavior is characteristic of endothermic adsorption kinetics, in which the initial rapid uptake is governed by film diffusion and abundant unsaturated surface sites, yielding high removal rates at early contact times. The slower second phase reflects intraparticle diffusion limitations, as dye molecules must diffuse into smaller pores or binding sites deeper in the biochar matrix (Wasilewska et al., 2024). The equilibrium plateau occurs when site saturation is approached and the driving concentration gradient becomes minimal; therefore, extending the contact time beyond 60 min yields negligible additional removal (Li et al., 2023). This time is lower than that reported in previous studies using industrial biochar for dye adsorption for 3 h (Jellali et al., 2022), 8 h (Yin et al., 2022), and 24 h (Fan et al., 2017). Having low equilibrium contact is one of an important aspect when considering scaling up as it reduces the energy consumption and treatment in real time.

3.2.4. Influence of dye concentration on Red F2B adsorption

The efficiency of dye removal by hydrochar derived from industrial sludge significantly decreased as the initial dye concentration increased. At a concentration of 5 mg/L, the

hydrochar removed 99.63% of the substance. However, at dye concentrations of 10 mg/L and 15 mg/L, the removal efficiency sharply declined to 59.25% and 58.87%, respectively, and further dropped to 37.96% at 20 mg/L (**Figure 99**). This behavior is typical of fixed site adsorption systems. At low initial concentrations, the number of dye molecules was low compared to the abundant active sites available on the hydrochar surface, enabling nearly all dye molecules to be captured. When the dye concentration increases, a greater number of molecules compete for the same limited adsorption sites, resulting in partial saturation of these sites and a subsequent reduction in the percentage of removal (Phuong et al., 2019).

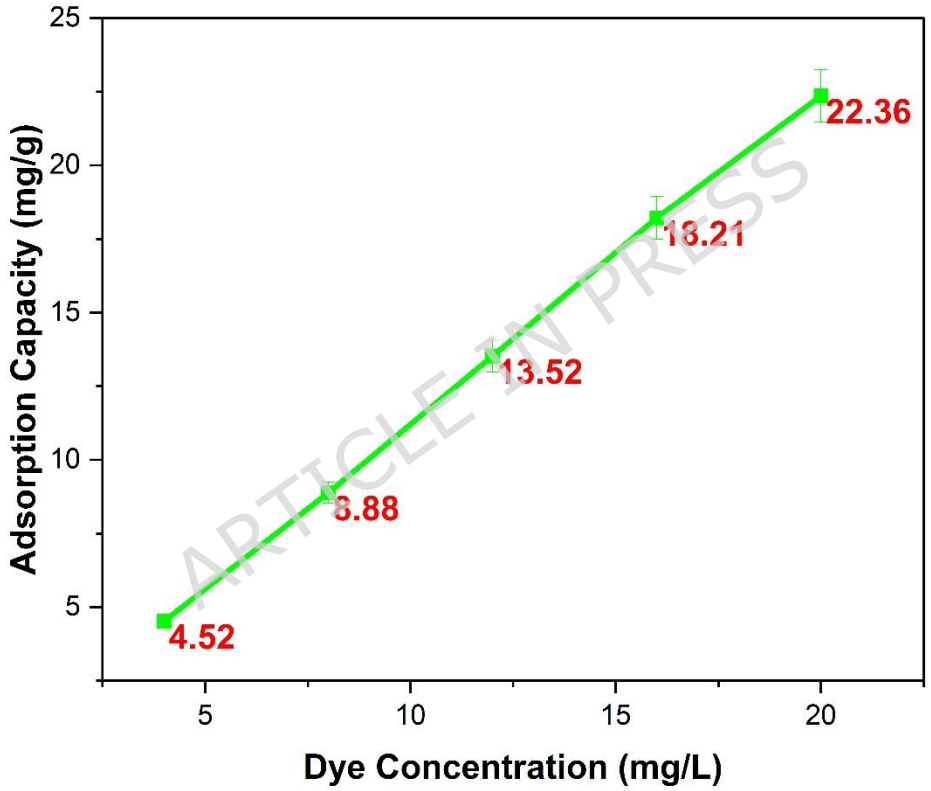

Figure 9. Influence of dye concentration on Red F2B adsorption

The results suggest that for effective dye removal using hydrochar derived from sludge, treatment systems should either function at relatively low incoming dye concentrations or be equipped with an adequate amount of hydrochar to ensure high removal efficiency, even when dye levels are high.

3.2.5. Influence of hydrochar concentration on adsorption of Red F2B dye

The removal efficiency of Red F2B dye by industrial sludge-derived hydrochar increased markedly with increasing adsorbent dosage. When the hydrochar concentration was raised from 0.2 g L^{-1} to 0.8 g L^{-1}, the dye removal percentage sharply increased from 20.22% to 85.55% (**Figure *10*10**). This behavior mirrors the trend observed in other hydrochar–dye systems, where increasing adsorbent dose provides more surface area and active binding sites, thus enhancing pollutant uptake (Saraswathi et al., 2023).

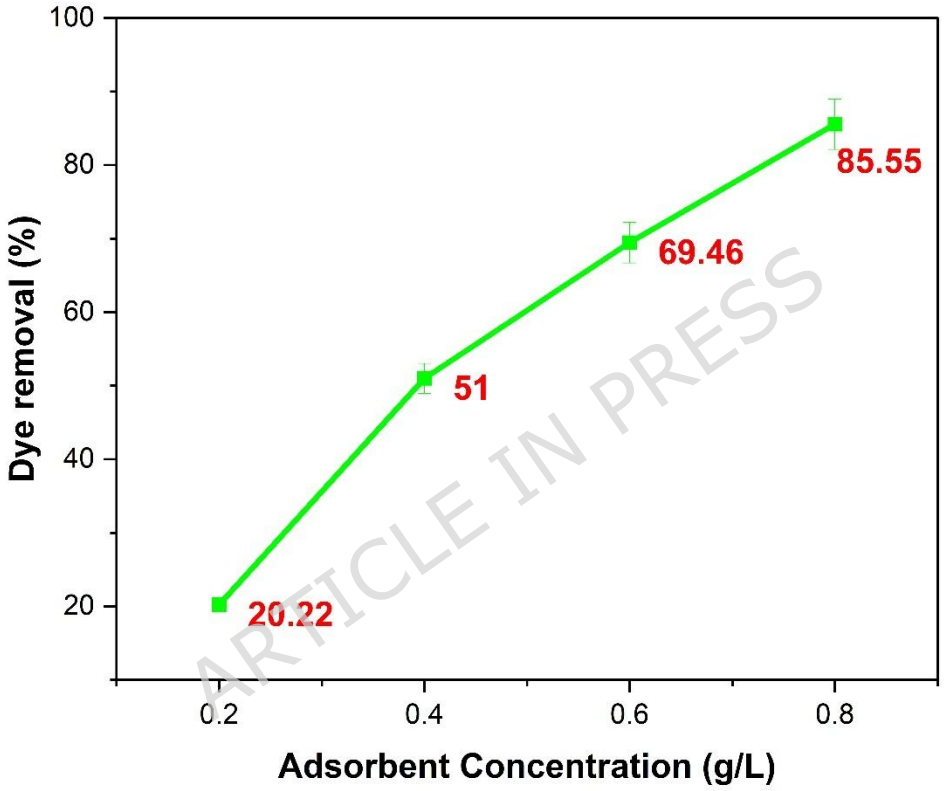

Figure 10. Influence of hydrochar concentration on adsorption of Red F2B dye

At low dosages (≤ 0.2 g L^{-1}), the limited number of adsorption sites leads to low removal efficiency because most of the dye molecules remain in solution. Increasing the dosage increased the available binding area, resulting in increased removal efficiency. At 0.8 g L^{-1}, the hydrochar provided sufficient active regions to capture the majority of dye molecules, achieving 85.55% removal before reaching equilibrium. Beyond the optimal dose, further increases in adsorbent concentration often yield diminishing returns or slight decreases in efficiency due to particle agglomeration and overlap of adsorption sites, which reduce the effective surface area available for sorption (Kayranli, 2025).

3.3. Adsorption Isotherm

The equilibrium adsorption data of Red F2B dye on industrial sludge-derived hydrochar were analyzed using three common isotherm models: LI, FI, and TI (**Figure *11*1**). The fitted parameters and statistical indicators are summarized in **Table *2*Table *3***.

The LI model showed the highest coefficient of determination (R^2 = 0.9709), suggesting an excellent fit of the data to the assumption of monolayer adsorption on a uniform surface at the adsorption sites. The maximum adsorption capacity (q_{max}) determined by LI was 44.24 mg g^{-1}, indicating a substantial capacity of the hydrochar to adsorb Red F2B dye. All R_L values lie between 0 and 1, indicating that the adsorption of Red F2B dye onto hydrochar was favorable at all initial concentration. The Freundlich constants indicated favorable adsorption (n ≈ 0.96) on a heterogeneous surface with moderate correlation (R^2 = 0.938). The TI model, which incorporates adsorbent–adsorbate interactions and heat of adsorption, exhibited the lowest fit quality (R^2 = 0.9149) and the highest reduced chi-square, suggesting lesser suitability for describing the system.

Isotherm analysis revealed Red F2B adsorption onto hydrochar derived from sludge predominantly adhered to the LI, indicating a monolayer adsorption process on a surface that is both homogeneous and energetically consistent. The relatively high maximum adsorption capacity (44.24 mg g^{-1}) demonstrates the effective dye uptake that can be achieved under the studied conditions. This capacity compares favorably with those of other biochars derived from industrial waste, underscoring the suitability of sludge-derived biochar for dye-remediation applications (Salim N. A. et al., 2021). The reasonable fit of the Freundlich isotherm suggests some degree of surface heterogeneity and multilayer adsorption, which is typical for hydrochar with diverse pore sizes and functional groups inherited from heterogeneous sludge feedstock. The Freundlich intensity parameter n, near 1, indicates that adsorption is nearly linear over the studied concentration range and slightly favors adsorption, consistent with physical adsorption processes. The TI model provided the poorest fit, suggesting that adsorbate–adsorbent interactions and variations in the heat of adsorption across sites have lesser impact on the overall adsorption process in this system than the other models (Dada et al., 2012). In summary, the predominance of Langmuir behavior confirmed that the adsorption sites on the sludge-derived hydrochar were finite and energetically equivalent, facilitating efficient monolayer coverage of the Red F2B dye molecules. This

insight aids in designing treatment processes by allowing estimation of hydrochar doses required for effective dye removal, given the saturation capacity.

Table 3. Isotherm Model Fitting Parameters for Red F2B Dye Adsorption onto activated Hydrochar

Langmuir Isotherm (LI)	
q_m	44.24 mg g^{-1}
b	0.358 L mg^{-1}
R^2	0.9709
Reduced Chi-square	2.94576
Adjusted R^2	0.9418
Freundlich Isotherm (FI)	
K_F	11.49 ((mg/g) $(L/mg)^{1/n}$
$1/n$	0.938
R^2	0.9623
Reduced Chi-square	2.5437
Adjusted R^2	0.9498
Temkin Isotherm (TI)	
B	10.61 ± 1.87 mg g^{-1}
A	3.43 ± 0.84 L g^{-1}
R^2	0.9149
Reduced Chi-square	5.7455
Adjusted R^2	0.8866

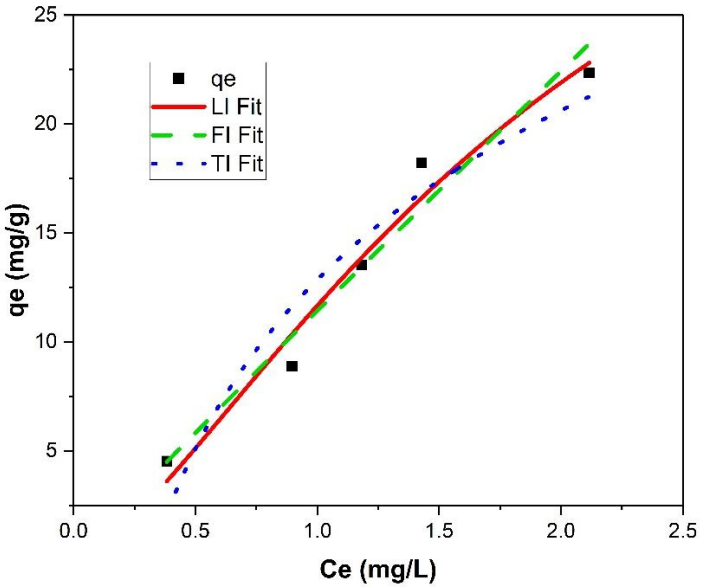

Figure 11. Langmuir, Freundlich, Temkin Isotherm Model Fitting Plot for the Adsorption of Red F2B Dye onto Activated hydrochar

The maximum Langmuir adsorption capacity (44.24 mg g^{-1}) achieved for Reactive Blue dye is comparable to several reported sludge-derived hydrochars and low-cost adsorbents. Sewage sludge hydrochars have exhibited capacities ranging between 38.6 and 87.0 mg g^{-1}, while $ZnCl_2$-activated pulp sludge hydrochar reported up to 590.2 mg g^{-1} for methylene blue (Zhao et al., 2021). Although activated carbons can achieve higher adsorption capacities (59.88–131.93 mg g^{-1}), and up to 1000 mg g^{-1} under optimized conditions, their production is associated with higher energy and reagent costs (Saleem et al., 2024) (Qian et al., 2024). Therefore, the current hydrochar's performance is considered competitive, particularly given its origin from waste sludge, minimal activation requirements, and the sustainability benefits associated with valorizing industrial sludge

3.4. Adsorption Kinetics

The kinetics of Red F2B dye adsorption onto hydrochar produced from industrial sludge were assessed using three models: pseudo-first-order (PFO), pseudo-second-order (PSO), and intraparticle diffusion (IPD) which were plotted in Fig. 12. A summary of the fitted parameters and goodness-of-fit metrics is provided in **Table *4***4

The high R^2 and adjusted R^2 values for both the PFO (0.969, 0.961) and PSO (0.963, 0.954) models indicated that each model could describe the adsorption kinetics well. The PFO model

yielded an equilibrium capacity (a) of ~7.31 mg g^{-1} and b of ~0.0299 min^{-1}, with reduced χ^2 of 0.1158, suggesting that early-stage adsorption is rapid and proportional to the number of unoccupied surface sites, consistent with physisorption mechanisms. However, the PFO model tends to underestimate uptake at longer contact times, indicating that the complete adsorption mechanism may not be fully captured (Rudzinski & Plazinski, 2008).

The PSO fit returned $q_e \approx 11.05$ mg g^{-1} and $k_2 \approx 0.00191$ g mg^{-1} min^{-1}, with reduced χ^2 of 0.1372. Despite a slightly lower R^2 than PFO, the PSO model provides a superior estimate of equilibrium capacity and is mechanistically consistent with **chemisorption**, suggesting that adsorption is controlled by electron sharing or exchange between dye molecules and functional groups on the hydrochar surface (Khamizov, 2020). The PSO rate constant indicates that ~90% of the equilibrium capacity is reached within ~47 min, highlighting rapid initial adsorption followed by slower approach to equilibrium, a characteristic of chemisorption processes

The IPD model exhibited $R^2 = 0.948$ (adjusted $R^2 = 0.935$) with a nonzero intercept (C = –1.275), indicating that intraparticle diffusion contributes to the adsorption process, but is not the sole rate-limiting step. The negative intercept suggests that film diffusion and boundary layer effects significantly influence the early adsorption stages, consistent with a two-step mechanism of rapid external adsorption followed by slower pore diffusion (Miyagawa et al., 2021).

Overall, these kinetic analyses revealed a composite mechanism: initial rapid physisorption onto external hydrochar surfaces, followed by chemisorption onto functional groups, with intraparticle diffusion modulating the later stages. These insights guide design of treatment units, indicating that ~60 min contact ensures near-equilibrium removal, and that enhancing intraparticle accessibility (e.g., via pore activation) could further improve uptake rates.

Table 4. Kinetic Model Fitting Parameters for Red F2B Adsorption on activated Hydrochar

PFO	
a	7.30804 ± 0.85623 mg g^{-1}
b	0.02989 ± 0.00687 min^{-1}
Reduced chi-square	0.11581
Coefficient of determination (R^2)	0.96878

Adjusted R^2	0.96098
PSO	
q_e	11.04545 ± 2.06736 mg·g^{-1}
K_2	0.00191 ± 0.00102 g·mg^{-1}·min^{-1}
R^2	0.96303
Adjusted R^2	0.95378
IPD	
K_{id}	0.987
C	−1.275
R^2	0.948
Adjusted R^2	0.935

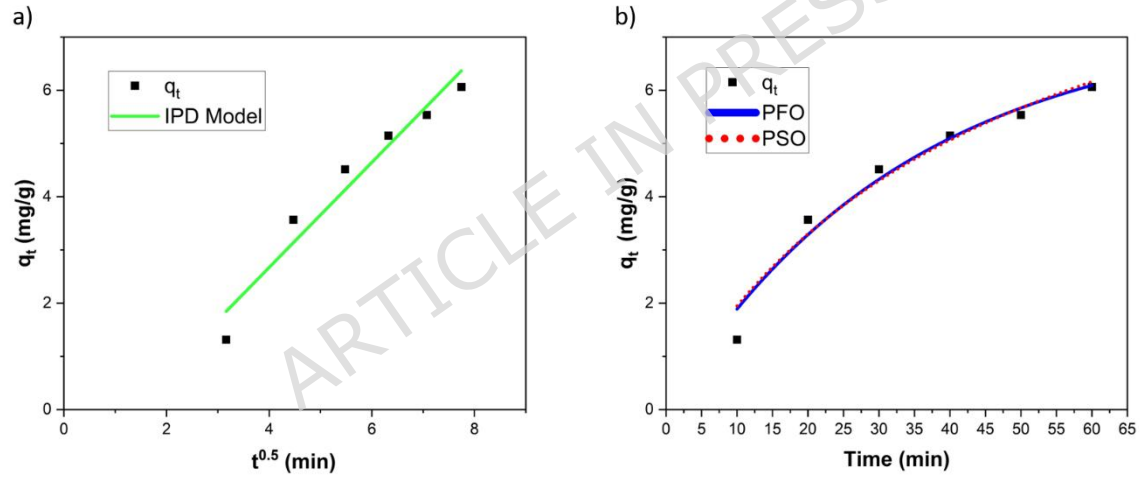

Figure 12. (a) IPD Model Fitting b) PFO and PSO Plot for the Adsorption of Red F2B onto Activated hydrochar

3.5. Thermodynamic Study

The thermodynamic parameters for the adsorption of Red F2B dye onto industrial sludge-derived hydrochar were calculated from Van't Hoff plots (ln Kd vs. 1/T) at four temperatures (303–333 K) were plotted in fig. 13. The changes in Gibbs free energy (ΔG°), enthalpy (ΔH°), and entropy (ΔS°) are shown in **Table *5***.

The gradual reduction in ΔG° as temperature rises suggests that elevated temperatures boost both the spontaneity and degree of Red F2B adsorption. This observation is consistent with

an endothermic process, where thermal energy aids the interaction between the dye and the adsorbent. The positive ΔH° value (46.33 kJ mol^{-1}) falls within the range typically associated with physical adsorption (<84 kJ mol^{-1}), yet it approaches the threshold where chemisorption contributions become significant, suggesting a combined mechanism involving hydrogen bonding and π–π interactions. The significant positive ΔS° (162.98 J mol^{-1} K^{-1}) indicates an increase in disorder, which is likely caused by the removal of water molecules from the hydrochar's porous surface as dye molecules take up the adsorption sites, along with potential structural changes in the surface moieties during binding. Such entropy-driven contributions further favour adsorption at high temperatures. In practical terms, the endothermic and spontaneous nature of Red F2B adsorption implies that operating treatment systems at moderately elevated temperatures (e.g., 333 K) will maximize removal efficiency. However, energy costs for heating must be balanced against gains in adsorption capacity. The thermodynamic parameters confirmed that sludge-derived hydrochar is a viable adsorbent for acidic dyes across different thermal conditions.

Table 5. Thermodynamic Study on Adsorption of Red F2B Dye onto Activated hydrochar

Temperature (K)	ΔG° (kJ/mol)	ΔH° (kJ/mol)	ΔS° (J/mol·K)
303	–2.97	46.33	162.98
313	–4.60		
323	–6.23		
333	–7.86		

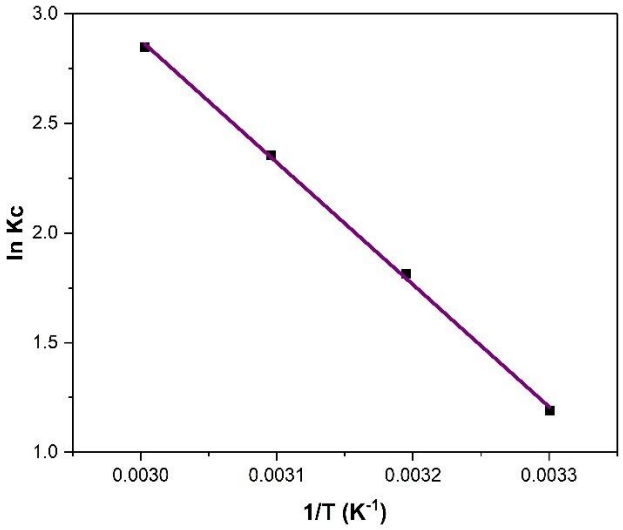

Figure 13. Van't Haff Thermodynamic Fitting

3.6. Adsorption mechanism

The adsorption of the Red F2B dye onto industrial sludge-derived hydrochar involves a combination of physisorption and chemisorption processes. FTIR analysis (Figure 3) confirmed the presence of oxygen-containing functional groups (O–H, C=O, C=C, and C–O) on the hydrochar surface, which served as active sites for adsorption via hydrogen bonding, electrostatic interactions, and π–π stacking (**Figure 14**). Kinetic studies have revealed that adsorption initially occurs rapidly on external surfaces (PFO fit) and gradually reaches equilibrium through chemisorption involving electron sharing or exchange with surface functional groups (PSO fit). Intraparticle diffusion (IPD model) contributes to the later stages, although film diffusion also affects the rate, indicating a multistep adsorption process. Isotherm analysis showed that adsorption predominantly follows the Langmuir model, indicating monolayer coverage on homogeneous, energetically similar sites, while the moderate Freundlich fit suggests some surface heterogeneity. Collectively, these findings demonstrate that sludge-derived hydrochar efficiently removes Red F2B dye through a combination of surface interactions and diffusion processes, thereby providing insights for optimizing adsorption-based treatment systems.

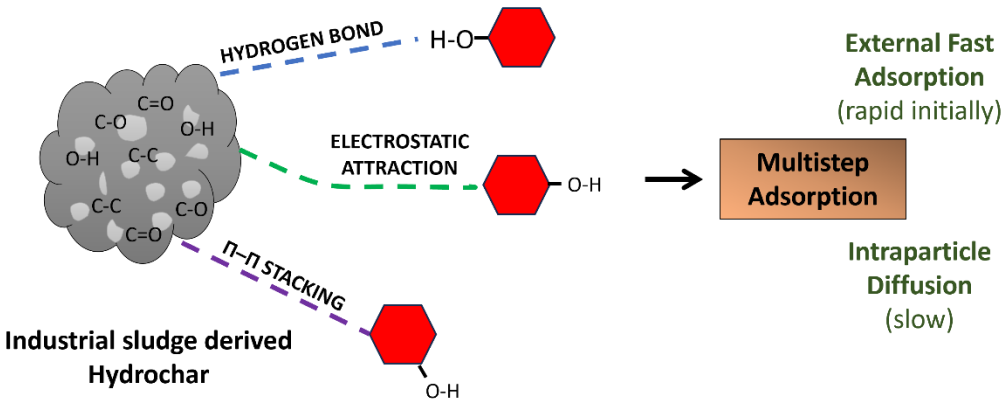

Figure 14. Schematic illustration of Red F2B adsorption on industrial sludge-derived hydrochar

3.7. Process Optimization using RSM

A Box-Behnken Design (BBD) was adopted, involving 35 experimental trials, to examine the individual and interactive effects of the selected parameters (**Table 6**)

Table 6. Parameters and observed removal efficiency of Red 2B dye

Run	pH	Temperature (kelvin)	Hydrochar Dosage (g/L)	Time (min)	Dye Concentration (mg/L)	Removal Efficiency (%)
1	3	333	0.8	60	5	83
2	5	333	0.8	60	5	62.4
3	7	333	0.8	60	5	62.8
4	3	333	0.8	10	5	21
5	3	333	0.8	20	5	57.12
6	3	333	0.8	30	5	72.21
7	3	333	0.8	40	5	82.4
8	3	333	0.8	50	5	88.6
9	3	333	0.8	60	5	97
10	3	303	0.8	60	5	72.4
11	3	313	0.8	60	5	83.1
12	3	323	0.8	60	5	89.4
13	3	333	0.8	60	5	93.2
14	3	333	0.2	60	5	20.2
15	3	333	0.4	60	5	51
16	3	333	0.6	60	5	69.5
17	3	333	0.8	60	5	85.5
18	3	333	0.8	10	10	14.4
19	3	333	0.8	20	10	17.5
20	3	333	0.8	30	10	17.6
21	3	333	0.8	40	10	43.2

22	3	333	0.8	50	10	59.1
23	3	333	0.8	60	10	59.2
24	3	333	0.8	10	20	14.1
25	3	333	0.8	20	20	13.8
26	3	333	0.8	30	20	13.7
27	3	333	0.8	40	20	13.6
28	3	333	0.8	50	20	13
29	3	333	0.8	60	20	12.4
30	7	333	0.8	10	5	36.7
31	7	333	0.8	20	5	42.3
32	7	333	0.8	30	5	16.4
33	7	333	0.8	40	5	25.2
34	7	333	0.8	50	5	27.4
35	7	333	0.8	60	5	17.1

The final regression equation obtained from the linear model, in terms of coded factors,

Removal Efficiency = -10.79 - 18.00A + 2.37B + 28.16C + 16.44D - 28.31E

The ANOVA findings for the linear model are shown in Table 7. With an F-value of 20.40 and a p-value less than 0.0001, the model is demonstrated to be statistically significant. This indicates that the model terms effectively captured the variation in removal efficiency. Among the five independent variables, pH (A)**,** hydrochar dosage (C)**,** contact time (D)**,** and initial dye concentration (E) were found to be significant ($p < 0.05$), whereas temperature (B) was not significant ($p > 0.1$), indicating a minimal effect on the removal efficiency within the studied range. The Lack of Fit (LOF) F-value was 0.74 with a p-value of 0.7184, indicating it was not significant. This implies that the model accurately represented the experimental data. A non-significant LOF is preferred because it shows that the model's predictions align well with the actual observations.

Table 7. ANOVA for Linear model

Source	Sum of Squares	df	Mean Square	F-value	p-value	
Model	23338.76	5	4667.75	20.40	< 0.0001	significant
A-pH	5760.07	1	5760.07	25.17	< 0.0001	
B-Temperature	27.35	1	27.35	0.1195	0.7320	
C-Hydrochar	3860.30	1	3860.30	16.87	0.0003	

Dosage						
D-Time	4124.95	1	4124.95	18.03	0.0002	
E-Dye concentration	11597.12	1	11597.12	50.68	< 0.0001	
Residual	6635.78	29	228.82			
Lack of Fit	5461.73	25	218.47	0.7443	0.7184	not significant
Pure Error	1174.05	4	293.51			
Cor Total	29974.53	34				

Statistical analysis of the RSM model yielded an R^2 value of 0.77 and a CV% of 32%, indicating a moderate degree of fit and relatively high experimental variability. The R^2 value, which is below the commonly accepted threshold of 0.90, suggests that the model accounts for 77% of the variability in the observed data, with a notable proportion of the variation remaining unexplained. This limitation may be attributed to the inherent complexity and heterogeneity of hydrochar-based adsorption systems, the possible exclusion of minor influential variables, and experimental noise. Given the relatively high CV%, the predictive ability of the model should be interpreted cautiously. Therefore, the current RSM fitting is best considered as a tool for guiding process optimization and understanding major trends rather than as a source of highly precise quantitative predictions. Future studies may improve the model accuracy and predictive power by incorporating additional variables, increasing the number of experimental runs, or employing more advanced modeling techniques.

The 3D surface plot (***Figure 155***) illustrates the combined influence of pH and temperature on the removal efficiency of Red F2B dye using HTC-derived hydrochar. The surface exhibited a mild inclination, confirming the linear nature of the model. Increasing pH led to a notable reduction in removal percentage, which is consistent with negative coefficient of pH (−18.00) in the regression equation and its statistical significance ($p < 0.0001$). This indicates that acidic environments promote adsorption, probably due to the increased electrostatic attraction between adsorbent and adsorbate molecules. In contrast, temperature appeared to have a minimal effect, as supported by its low regression coefficient (+2.37) and high p-value ($p = 0.73$) from ANOVA. The surface showed only slight variation along the temperature axis, reinforcing that temperature is not a dominant factor in this process within the tested range.

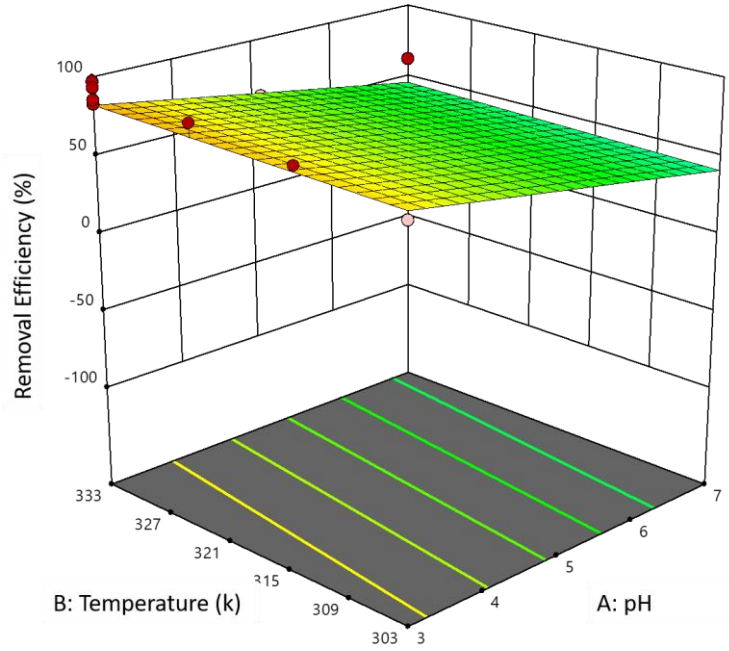

Figure 15. A 3D graph illustrating the impact of temperature and pH on the efficiency of Red F2B removal

4. Conclusion

This research demonstrates the effective synthesis and application of hydrochar derived from industrial sludge through hydrothermal carbonization to eliminate Red F2B dye from aqueous solutions. Hydrochar exhibits favorable physicochemical properties, including a porous structure, diverse surface functional groups, and heterogeneous composition, which contribute to its adsorption capabilities. The adsorption process was influenced by the pH level, achieving the highest removal efficiency at an acidic pH of 3. Temperature positively influenced dye uptake, indicating an endothermic process. The adsorption kinetics followed a two-stage pattern, with rapid initial uptake, followed by a slower approach to equilibrium. The adsorption equilibrium was most accurately represented by the LI, indicating monolayer adsorption on a uniform surface with a peak adsorption capacity of 44.24 mg g^{-1}. Kinetic investigations indicated that the PSO was the most accurate, suggesting that chemisorption was the step that limited the rate. Thermodynamic evaluation verified that the adsorption process was both spontaneous and endothermic, with spontaneity increasing as the temperature rose. Response Surface Methodology optimization identified pH, hydrochar dosage, contact time, and initial dye concentration as significant factors affecting the removal efficiency. The developed model showed only a moderate predictive capability, and its results should be interpreted with caution for Red F2B dye removal. In conclusion, these results

highlight the potential of industrial sludge-derived hydrochar as an effective and sustainable adsorbent for dye removal from wastewater, providing valuable insights into the adsorption mechanisms of the material and guiding future applications in water treatment.

Recommendation for future work

Based on the findings of this research, subsequent studies should aim to improve the practical use of hydrochar derived from HTC in the treatment of wastewater. Expanding the process to a larger scale and performing pilot-scale studies will provide essential insights into the operational viability and real-world effectiveness of the adsorbent in industrial settings. Examining the regeneration and reuse of hydrochar over several cycles is crucial for evaluating its long-term cost efficiency. Furthermore, competitive adsorption tests with actual textile effluents or multi-component dye systems are necessary to replicate real wastewater conditions. Exploring methods for altering surfaces, like chemical activation or functionalization, may enhance the adsorption capacity and selectivity of hydrochar. It is advisable to conduct a comprehensive life cycle assessment (LCA) to evaluate the environmental sustainability of this approach in comparison to conventional treatment methods. To enhance mechanistic understanding, advanced analytical methods can be used to elucidate the adsorption mechanisms at the molecular level. Additionally, optimizing the HTC parameters to customize surface properties and extending the research to other pollutants, such as heavy metals, pharmaceuticals, and emerging contaminants, would expand the material's applicability. Continuous flow experiments and economic feasibility studies are essential for transforming this lab-scale innovation into a scalable, sustainable solution for industrial wastewater treatment.

Declarations

Ethical approval: Not applicable.

Consent to participate: All the authors participated in this study.

Consent for publication: All authors agree to publish this manuscript.

Authors Contributions:

B. Senthil Rathi: Conceptualization; Investigation; Methodology; Validation; Writing original-draft

P. Senthil Kumar, Gayathri Rangasamy: Conceptualization; Investigation; Methodology; Validation; Supervision

S. Murugeshwari, K. Sathish Kumar, S. Meenakshi Lalitha: Conceptualization; Visualization; Formal Analysis; Data curation

Funding: This study did not receive financial support.

Competing Interests: The authors declare that they have no competing interests

Availability of data and materials: All data generated or analyzed during this study are included in this published article.

Reference

1. Ali, A. C., Saleem, H. M., & Akhter, A. (2023). Physiological and biochemical characterization of biochar-induced resistance against bacterial wilt of eggplant. *Royal Society Open Science, 10*(2), 230442. https://doi.org/https://doi.org/10.1098/rsos.230442

2. Al-Saeedi, S. I., Asfa, A., Qamar, M. T., Alhujaily, A., Iqbal, S., Alotaibi, M. T., Aslam, M., Qayyum, M. A., Bahadur, A., Awwad, N. S., Jazaa, Y., & Elkaeed, E. B. (2023). Isotherm and kinetic studies for the adsorption of methylene blue onto a novel Mn_3O_4-Bi_2O_3 composite and their antifungal performance. *Frontiers in Environmental Science, 11*(Article 1156475). https://doi.org/https://doi.org/10.3389/fenvs.2023.1156475

3. Andersen, S. I., Jensen, J. O., & Speight, J. G. (2005). X-ray Diffraction of Subfractions of Petroleum Asphaltenes. . *Energy & Fuels, 19*(6), 2371–2377. https://doi.org/https://doi.org/10.1021/ef050039v

4. Budnyak, T. M., Błachnio, M., Slabon, A., Jaworski, A., Tertykh, V. A., Deryło-Marczewska, A., & Marczewski, A. W. (2020). Chitosan Deposited onto Fumed Silica Surface as Sustainable Hybrid Biosorbent for Acid Orange 8 Dye Capture: Effect of Temperature in Adsorption Equilibrium and Kinetics. *The journal of physical chemistry. C, Nanomaterials and interfaces, , 124*(28), 15312–15323. https://doi.org/https://doi.org/10.1021/acs.jpcc.0c04205

5. Cano, F. J., González Reyes, M., Cruz-Salomón, A., Montejo-López, W., Sánchez-Albores, R. M., Serrano Ramirez, R. D., Torres-Ventura, H. H., Hernández-Cruz, M. D., Reyes-Vallejo, O., & Sebastian, P. J. (2024). Activated Biochar from Pineapple Crown Biomass: A High-Efficiency Adsorbent for Organic Dye Removal. . *Sustainability, 17*(1), 99. https://doi.org/https://doi.org/10.3390/su17010099

6. Chang, Y., Yang, D., Li, R., Wang, T., & Zhu, Y. (2021). Textile Dye Biodecolorization by Manganese Peroxidase: A Review. *Molecules, 26*(15), 4403. https://doi.org/https://doi.org/10.3390/molecules26154403

7. Chen, C., Liang, W., Fan, F., & Wang, C. (2021). The Effect of Temperature on the Properties of Hydrochars Obtained by Hydrothermal Carbonization of Waste Camellia oleifera Shells. . *ACS omega, 6*(25), 16546–16552. https://doi.org/https://doi.org/10.1021/acsomega.1c01787

8. Fahmi, A. H., Samsuri, A. W., Jol, H., & Singh, D. (2018). Physical modification of biochar to expose the inner pores and their functional groups to enhance lead adsorption. . *RSC advances, 8*(67), 38270–38280. https://doi.org/https://doi.org/10.1039/c8ra06867d

9. Graça, N. S., & Rodrigues, A. E. (2022). The Combined Implementation of Electrocoagulation and Adsorption Processes for the Treatment of Wastewaters. . *Clean Technologies, 4*(4), 1020–1053. https://doi.org/ https://doi.org/10.3390/cleantechnol4040063

10. Hossain, N., Nizamuddin, S., & Griffin, G. e. (2020). Synthesis and characterization of rice husk biochar via hydrothermal carbonization for wastewater treatment and biofuel production. *Sci Rep, 10*, 18851. https://doi.org/https://doi.org/10.1038/s41598-020-75936-3

11. Jellali, S., Azzaz, A. A., Al-Harrasi, M., Charabi, Y., Al-Sabahi, J. N., Al-Raeesi, A., Usman, M., Al Nasiri, N., Al-Abri, M., & Jeguirim, M. (. (2022). Conversion of Industrial Sludge into Activated Biochar for Effective Cationic Dye Removal: Characterization and Adsorption Properties Assessment. *Water, 14*(14), 2206. https://doi.org/https://doi.org/10.3390/w14142206

12. Jian, X., Zhuang, X., Li, B., Xu, X., Wei, Z., Song, Y., & Jiang, E. (2018). Comparison of characterization and adsorption of biochars produced from hydrothermal carbonization and pyrolysis. *Environmental Technology & Innovation, 10*, 27–35. https://doi.org/https://doi.org/10.1016/j.eti.2018.01.004

13. Kapoor, R. T., Khan, M. A., Sillanpää, M., Rafatullah, M., & Siddiqui, M. R. (2022). Removal of Reactive Black 5 Dye by Banana Peel Biochar and Evaluation of Its Phytotoxicity on Tomato. *Sustainability, 14*(7), 4176. https://doi.org/https://doi.org/10.3390/su14074176

14. Kayranli, B. (2025). Adsorption efficiency of groundnut husk biochar in reduction of rhodamine B, recycle, and reutilization. . *Biomass Conversion and Biorefinery*. https://doi.org/https://doi.org/10.1007/s13399-025-06781-5

15. Khamizov, R. K. (2020). A Pseudo-Second Order Kinetic Equation for Sorption Processes. *Russian Journal of Physical Chemistry A, 94*(1), 171–176. https://doi.org/https://doi.org/10.1134/s0036024420010148

16. Khan, H., Yerramilli, A. S., D'Oliveira, A., Alford, T. L., Patience, G. S., & Boffito, D. C. (2020). Experimental methods in chemical engineering: X-ray diffraction spectroscopy—

XRD. *The Canadian Journal of Chemical Engineering, 98*(6), 1255–1266. https://doi.org/https://doi.org/10.1002/cjce.23747

17. Li, P., Zhao, T., Zhao, Z., Tang, H., Feng, W., & Zhang, Z. (2023). Biochar derived from Chinese herb medicine residues for Rhodamine B dye adsorption. *ACS Omega, 8*(5), 4813–4825. https://doi.org/https://doi.org/10.1021/acsomega.2c06968

18. Liang, H., Chen, L., Liu, G., & Zheng, H. (2016). Surface morphology properties of biochars produced from different feedstocks. *In Proceedings of the 2016 International Conference on Civil, Transportation and Environment.* Atlantis Press. https://doi.org/10.2991/iccte-16.2016.210

19. Libra, J. A., Ro, K. S., Kammann, C., Funke, A., Berge, N. D., Neubauer, Y., & … Emmerich, K. H. (2011). Hydrothermal carbonization of biomass residuals: a comparative review of the chemistry, processes and applications of wet and dry pyrolysis. *Biofuels, 2*(1), 71–106. https://doi.org/https://doi.org/10.4155/bfs.10.81

20. Liu, C., Huang, X., & Kong, L. (2017). Efficient Low Temperature Hydrothermal Carbonization of Chinese Reed for Biochar with High Energy Density. *Energies, 10*(12), 2094. https://doi.org/https://doi.org/10.3390/en10122094

21. Luba, M., Mikołajczyk, T., Kuczyński, M., Pierożyński, B., Jasiecka-Mikołajczyk, A., Rasiński, B., & Wojtacha, P. (2023). Electrochemical purification of Disperse Red 167 azo dye-based synthetic wastewater through the electrooxidation and electrocoagulation with Fe ions derived from Cu/Fe macro-corrosion galvanic cell. *Desalination and Water Treatment, 287*, 67–79. https://doi.org/https://doi.org/10.5004/dwt.2023.29355

22. Mccall, M. A., Watson, J. S., & Sephton, M. A. (2024). Predicting Stability of Barley Straw-Derived Biochars Using Fourier Transform Infrared Spectroscopy. *ACS Sustainable Resource Management, 1*(9), 1975–1983. https://doi.org/https://doi.org/10.1021/acssusresmgt.4c00148

23. Miyagawa, A., Nakatani, K., Kazami, H., Terada, T., & Nagatomo, S. (2021). Kinetic Analysis of the Mass Transfer of Zinc Myoglobin in a Single Mesoporous Silica Particle by Confocal Fluorescence Microspectroscopy. *Langmuir, 37*(43), 12697–12704. https://doi.org/https://doi.org/10.1021/acs.langmuir.1c02127

24. Pasieczna-Patkowska, S., Cichy, M., & Flieger, J. (2025). Application of Fourier Transform Infrared (FTIR) Spectroscopy in Characterization of Green Synthesized Nanoparticles. . *Molecules (Basel, Switzerland), 30*(3), 684. https://doi.org/https://doi.org/10.3390/molecules30030684

25. Pereira, L., & Alves, M. (2012). Dyes-Environmental Impact and Remediation. In *Environmental Protection Strategies for Sustainable Development* (p. 111−162). Springer Netherlands.

26. Petrovic, J., Ercegović, M., Simić, M., Koprivica, M., Dimitrijević, J., Jovanović, A., & Janković Pantić, J. (2024). Hydrothermal Carbonization of Waste Biomass: A Review of

Hydrochar Preparation and Environmental Application. *Processes, 12*(1), 207. https://doi.org/https://doi.org/10.3390/pr12010207

27. Phuong, D. T., Loc, N. X., & Miyanishi, T. (2019). Efficiency of dye adsorption by biochars produced from residues of two rice varieties, Japanese Koshihikari and Vietnamese IR50404. . *Desalination and Water Treatment, 165*, 333–351. https://doi.org/https://doi.org/10.5004/dwt.2019.24496

28. Qambrani, N. A., Rahman, M. M., Won, S., Shim, S., & Ra, C. (2017). Biochar properties and eco-friendly applications for climate change mitigation, waste management, and wastewater treatment: A review. *Renewable and Sustainable Energy Reviews, 79*, 255–273. https://doi.org/https://doi.org/10.1016/j.rser.2017.05.057

29. Routoula, E., & Patwardhan, S. V. (2020). Degradation of Anthraquinone Dyes from Effluents: A Review Focusing on Enzymatic Dye Degradation with Industrial Potential. *Environmental science & technology, 54*(2), 647–664. https://doi.org/https://doi.org/10.1021/acs.est.9b037

30. Rudzinski, W., & Plazinski, W. (2008). Kinetics of Solute Adsorption at Solid/Aqueous Interfaces: Searching for the Theoretical Background of the Modified Pseudo-First-Order Kinetic Equation. *Langmuir, 24*(10), 5393–5399. https://doi.org/https://doi.org/10.1021/la8000448

31. Salim, N. A., Puteh, M. H., Khamidun, M. H., Fulazzaky, M. A., Abdullah, N. H., Yusoff, A. R., Zaini, M. A., Ahmad, N., Lazim, Z. M., & Nuid, M. (2021). Interpretation of isotherm models for adsorption of ammonium onto granular activated carbon. *Biointerface Research in Applied Chemistry, 11*(2), 9227–9241. https://doi.org/https://doi.org/10.33263/BRIAC112.92279241

32. Saraswathi, R., Praveen, S., & Nithyalakshmi, B. (2023). Removal of Basic Fuchsin Red dye by Turmeric leaf waste biochar: Batch adsorption studies, isotherm kinetics and RSM studies. *Global NEST Journal, 25*(1). https://doi.org/https://doi.org/10.30955/gnj.004443

33. Smoczyński, L., Pierożyński, B., & Mikołajczyk, T. (2020). The Effect of Temperature on the Biosorption of Dyes from Aqueous Solutions. *Processes, 8*(6), 636. https://doi.org/https://doi.org/10.3390/pr8060636

34. Sukmana, H., Hodur, C., Pantoja, F., & Bellahsen, N. (2021). Adsorption and coagulation in wastewater treatment – Review. . *Progress in Agricultural Engineering Sciences, 17*(1), 49–68. https://doi.org/https://doi.org/10.1556/446.2021.00029

35. Tu, W., & Cai, W. (2024). Selective Adsorption of Hazardous Substances from Wastewater by Hierarchical Oxide Composites: A Review. *Toxics, 12*(7), 447. https://doi.org/https://doi.org/10.3390/toxics12070447

36. Vaghela, S. S., Jethva, A. D., Mehta, B. B., Dave, S. P., Adimurthy, S., & Ramachandraiah, G. (2005). Laboratory studies of electrochemical treatment of industrial azo dye effluent. *Environmental science & technology, 39*(8), 2848–2855. https://doi.org/https://doi.org/10.1021/es035370c

37. Veiga, T. R., Trugilho, P. F., Dessimoni, A. L., Pego, M. F., Lima, J. T., & & Soares, J. R. (2017). DIFFERENT PLANT BIOMASS CHARACTERIZATIONS FOR BIOCHAR PRODUCTION. *CERNE, 23*(4), 529–536. https://doi.org/https://doi.org/10.1590/01047760201723042373

38. Wang, W., Chen, W.-H., & J. M.-F. (2020). Characterization of Hydrochar Produced byHydrothermal Carbonization of Organic Sludge. *Future Cities andEnvironment, 6(1)*(13), 1–10. https://doi.org/https://doi.org/10.5334/fce.102

39. Wasilewska, M., Derylo-Marczewska, A., & Marczewski, A. W. (2024). Comprehensive Studies of Adsorption Equilibrium and Kinetics for Selected Aromatic Organic Compounds on Activated Carbon. . *Molecules (Basel, Switzerland), 29*(9), 2038. https://doi.org/https://doi.org/10.3390/molecules29092038

40. Yoo, S., Park, S., Kelley, S. S., & Tilotta, D. C. (2018). Structural Characterization of Loblolly Pine Derived Biochar by X-ray Diffraction and Electron Energy Loss Spectroscopy. *ACS Sustainable Chemistry & Engineering, 6*(2), 2621–2629. https://doi.org/https://doi.org/10.1021/acssuschemeng.7b04119

41. Zahuri, A. A., Abdul Patah, M. F., Kamarulzaman, Y., Hashim, N. H., Thirumoorthi, T., Wan Mohtar, W. H., Mohd Hanafiah, Z., Amir, Z., & Wan-Mohtar, W. A. (2023). Decolourisation of Real Industrial and Synthetic Textile Dye Wastewater Using ActActivated Dolomite. *Water, 15*(6), 1172. https://doi.org/https://doi.org/10.3390/w15061172

42. Zhang, L., Gonçalves, A. A., & Jaroniec, M. (2020). Identification of preferentially exposed crystal facets by X-ray diffraction†. *RSC Advances, 10*(10), 5585–5589. https://doi.org/https://doi.org/10.1039/d0ra00769b

43. Zhao, L., Sun, Z. F., Pan, X. W., Tan, J. Y., Yang, S. S., Wu, J. T., Chen, C., Yuan, Y., & Ren, N. Q. (2023). Sewage sludge derived biochar for environmental improvement: Advances, challenges, and solutions. *Water research X, 18*, 100167. https://doi.org/https://doi.org/10.1016/j.wroa.2023.100167

44. Zhou, Y., Ni, H., Fang, D., Yang, X., Qi, J., Yang, Y., Zhu, Z., Zhou, L., Li, J., & Gao, J. (2024). Recent Progress in Sludge-Derived Biochar and Its Role in Wastewater Purification. *Sustainability, 16*(12), 5012. https://doi.org/https://doi.org/10.3390/su16125012